NUCLEAR SCIENCE AND ENGINEERING

DOI: https://doi.org/10.1080/00295639.2019.1570750

Tantalum, Titanium, and Zirconium Neutron Total Cross-Section Measurements from 0.4 to 25 MeV

M. J. Rapp,*[a] D. P. Barry,[a] G. Leinweber,[a] R. C. Block,[a] B. E. Epping,[a] T. H. Trumbull,[a] and Y. Danon[b]

[a]*Naval Nuclear Laboratory, P.O. Box 1072, Schenectady, New York 12301-1072*
[b]*Rensselaer Polytechnic Institute, Department of Mechanical, Aerospace, and Nuclear Engineering, 110 8th Street, Troy, New York 12180-3590*

Received September 10, 2018
Accepted for Publication January 13, 2019

Abstract — *The electron linear accelerator housed in the Gaerttner Linear Accelerator Center at Rensselaer Polytechnic Institute was used to generate a pulsed neutron source to measure the neutron total cross section of tantalum, titanium, and zirconium from 0.4 to 25 MeV. Neutron transmission measurements were made using the time-of-flight method with neutron flight paths of approximately 100 and 250 m. The long flight paths combined with narrow neutron pulse widths, fast detector responses, fast electronics, and data collection system provide good energy resolution for the measurements. A high signal-to-background ratio through much of the energy range combined with low statistical errors resulted in low uncertainties on cross sections.*

The results are presented and compared with the major nuclear data evaluations. Each measurement identifies regions where the neutron total cross sections could be reevaluated. The total cross-section measurements presented here can help nuclear data evaluators improve neutron total cross-section data in future evaluations.

Keywords — *Cross section, transmission, tantalum, titanium, zirconium.*

Note — *Some figures may be in color only in the electronic version.*

I. INTRODUCTION

The three materials measured—tantalum, titanium, and zirconium—have characteristics that are desirable for use in nuclear systems. As such, a precise knowledge of their neutron cross sections and uncertainties is essential for accurate neutron transport calculations. Tantalum is a dense metal with extremely high melting temperature (3017°C), only exceeded by osmium, rhenium, and tungsten. Because of this high melting temperature, as well as good mechanical properties, it has been investigated for use in fusion applications as a first-wall and structural material.[1] Titanium has a low density and high strength-to-weight ratio as well as a high resistance to corrosion. These properties make it desirable for nuclear systems concerned with transport and storage containers.[2] Zirconium and zirconium alloys possess a mix of good mechanical properties and low thermal absorption cross section. For these reasons, they are a common choice for fuel cladding as well as primary systems structural material in both light and heavy water reactors.[3]

II. METHODS

II.A. Experimental Setup

The electron linear accelerator (linac) housed in the Rensselaer Polytechnic Institute (RPI) Gaerttner Linear Accelerator Center was used to create short pulses of neutrons. The L-band linac injects packets of highly energetic electrons (~55 MeV) onto a neutron producing target, which consists of several water-cooled tantalum

*E-mail: rappm@rpi.edu

plates in an aluminum housing.[4] The high-energy electrons from the linac generate bremsstrahlung X-rays within the target, which subsequently interact with the tantalum via (γ, n) reactions to produce photoneutrons. These interactions generate a continuous energy neutron source which can be approximated by an evaporation spectrum with a temperature of 0.55 MeV (Ref. 5). The neutrons migrate through evacuated neutron flight path drift tubes to a neutron detection system. Along the flight path gamma rays are filtered using depleted uranium and neutrons are collimated using a series of lead, boron carbide, polyethylene, and iron collimators. An overview of the experimental setup is shown in Fig. 1. Due to the pulsed nature of the neutron production, the energy of the neutrons reaching the detector could be calculated using a relativistic neutron time-of-flight (TOF) method.[6]

The detector was a modular proton recoil detector, comprised of two custom designed EJ-301 liquid scintillation detector modules.[6] Each of the modules is 17.8 cm high, 35.1 cm wide, and 12.7 cm thick. Two Photonis XP4572B 12.7-cm-diameter photomultiplier tubes were coupled to each module to optimize light collection. The two modules were combined to give the detector a neutron beam measurement cross section of 35.6 × 35.1 cm. The analog signals from the photomultiplier tubes were conditioned by collecting the output pulses from the detector and converting them to logic pulses using an ORTEC 935 constant fraction discriminator, which allowed for optimizing time resolution over the wide range of pulse amplitudes. The responses from the two detectors were then summed in an ORTEC CO4020 logic unit. These electronics were located locally at either the 100-m flight station or the 250-m flight station, depending on the experiment being performed, to prevent significant signal degradation through long transmission lines. The logic pulses were transmitted by fiber optics from the flight station to the data acquisition system (DAQ) located in the Gaerttner Center control room. The data were recorded in either 1.6- or 3.2-ns time bins using a FastComTec P7889 multiscaler board. The P7889 is a 10-GHz TOF clock with no dead time between channels capable of <400 ps full-width at half-maximum jitter per 100 μs (Ref. 7). An overview of the electronics is shown in Fig. 2, which presents a signal flow diagram from the detector to the DAQ.

Additional neutron detectors were installed in an independent beam line at the linac facility, at a flight path of approximately 9 m, and were used to monitor the neutron flux emitted from the target. Two moderated fission chambers were used for the 100-m experiments, a Reuter-Stokes RS-P6-2403-121 and Amperex B300D. Three moderated fission chambers were installed for the

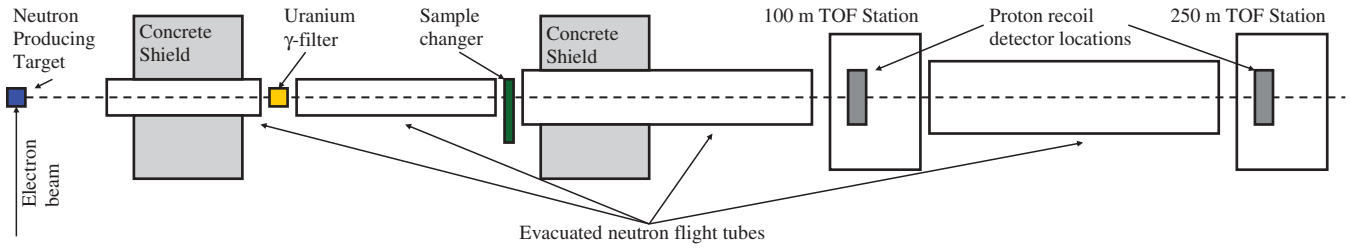

Fig. 1. Experimental setup showing the neutron-producing target, neutron flight paths, uranium filter location, sample position, and detector locations (not to scale).

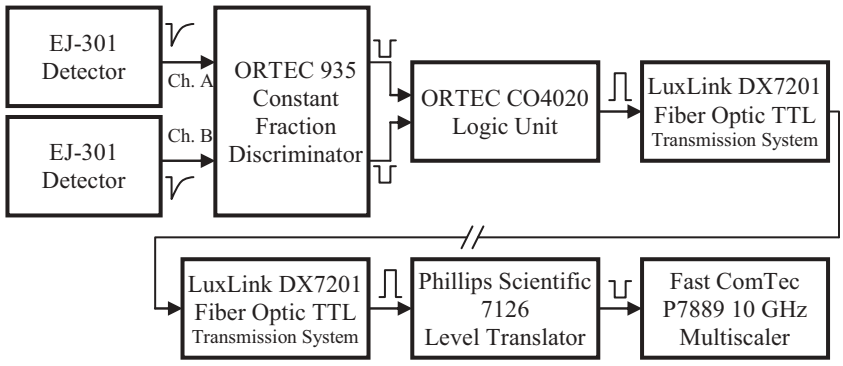

Fig. 2. Flow diagram of electronics used for data collection showing the signal path from detector to data collection at the TOF clock. The break between the two DX7201 transmission system units represents where the signal travels a long distance from the detector location at 100 or 250 m to the Gaerttner Center control room where data are collected.

250-m experiments, two Westinghouse WL6149A and one Amperex B300D.

Transmission measurements were conducted using the sample-in divided by sample-out method. Data for each material of interest (sample-in), open beam (sample-out), and carbon data were collected during each individual experiment. The carbon sample was a reference sample, used during each experiment to benchmark the system and verify the TOF-to-energy calibration. Carbon was selected as a reference due to the agreement between the major nuclear data libraries as well as sharp cross-section structure to align energy with. Data were typically collected over 50 to 80 h during each experiment. The time each sample and the open were measured was chosen to minimize the experiment time required to achieve reasonable statistics.[8] The basic experimental parameters for each material are outlined in Table I. The flight path represents the distance traveled by the neutrons from generation in the target to detection in the detector system. The uncertainty in the flight path is estimated from the ability to accurately replicate the energies of the structure seen in the carbon reference measurement. The channel width represents the time bins into which the P7889 clock records the data and is set in the clock options. The pulse width was the width of the neutron burst from the target recorded at the beginning of the TOF spectrum. A small burst width was prioritized when tuning the linac for each experiment and was generally the smallest achievable. The linac repetition rate was the frequency of electron pulses produced by the linac in pulses per second (pps). The beam time represents the total time that good data were being collected by the detector system.

For each experiment, data from both sample thicknesses listed in Table II, carbon, and open beam were collected into 100 to 200 individual data files. Each data file represented approximately 30 min of in-beam time. This was done to avoid the loss of large amounts of data in the event that corrupted data were generated during any single run, as well as enabling more accurate correction for instabilities in electron beam conditions. The data were reduced to transmission and converted to neutron total cross section.

II.B. Samples

The tantalum experiment was conducted using cylindrical samples of 99.95% pure tantalum. The two tantalum samples measured were 4 and 5.5 cm thick. The titanium experiment was conducted using two cylindrical samples of 99.99% pure titanium. The two titanium samples measured were 8 and 12 cm thick. The zirconium experiment was conducted using two cylindrical samples of 99.9% pure zirconium. The two zirconium samples measured were 6 and 10 cm thick. Each of the experiments used the same 13-cm-thick carbon reference sample, which was taken from 99.9% pure carbon stock.[9] All samples were machined to cylinders with diameters $\geq$7.5 cm to ensure neutron beam coverage at the sample changer location and maintain good experimental sample geometry. The sample characteristics are summarized in Table II.

II.C. Data Analysis

The individual experimental data files were summed, dead-time corrected, and written to a file useful for subsequent data analysis using an in-house analysis program, RPIXDR (Ref. 10). The code also produced an output file containing the neutron monitor data, integrated detector data, and various other data used for verification of run integrity for use in another custom code, MONCHK (Ref. 11). The MONCHK code performed statistical checks between sample data sets and monitor data sets, and reported any abnormalities for further examination.

The transmission T in each TOF channel was calculated from the measured sample-in and sample-out detector counts C^S and C^O, respectively, and the associated background B^S and B^O, as shown in Eq. (1):

TABLE I

Experimental Parameters for Each Transmission Measurement

Sample Material	Flight Path (m)	TOF Channel Width (ns)	linac Pulse Width (ns)	linac Repetition Rate (pps)	linac Beam Time (h)
Ta	99.95 ± 0.01	1.6	9.8	400	70.4
Ti	99.95 ± 0.01	1.6	9.2	400	75.9
Ti	249.74 ± 0.01	3.2	5.1	400	48.8
Zr	99.95 ± 0.01	1.6	8.0	400	78.4
Zr	249.74 ± 0.01	3.2	8.9	400	49.9

TABLE II

Sample Characteristics

Sample	Nominal Thickness (cm)	Diameter (cm)	Mass (g)	Areal Number Density (atoms/barn)
Tantalum	4	7.624 ± 0.001	3041.8 ± 0.1	0.22174 ± 0.00006
Tantalum	5.5	7.630 ± 0.001	4215 ± 1	0.3068 ± 0.0001
Titanium	8	7.693 ± 0.001	1728.5 ± 0.1	0.4679 ± 0.0001
Titanium	12	7.696 ± 0.001	2585.3 ± 0.1	0.6993 ± 0.0002
Zirconium	6	7.621 ± 0.001	1783.4 ± 0.1	0.25812 ± 0.00007
Zirconium	10	7.619 ± 0.001	2967.2 ± 0.1	0.4296 ± 0.0001
Carbon	13	7.498 ± 0.002	968.8 ± 0.1	1.1001 ± 0.0004

$$T = \left[\frac{C^S - B^S}{C^O - B^O}\right]\frac{mon^O}{mon^S} , \quad (1)$$

where the ratio of background subtracted counts was normalized using the sample-in and sample-out neutron beam monitor counts, mon^S and mon^O. The beam monitor counts used for normalization accounted for differences in neutron beam intensity between the sample and open experimental runs. The sample and open run summed data as well as monitor data were taken directly from the RPIXDR output files, while the background information had to be inferred from the data using the method described in Ref. 6.

The background is typically the most difficult parameter to accurately define in a transmission analysis. A constant background and a time-dependent portion are the two components that generally determine the background. The constant background is generated from natural radiation in the environment, such as earthen and building materials and cosmic radiation. This component was determined from the time recorded prior to the generation of neutrons and was consistent with recorded measurements taken without the linac in operation. The time-dependent portion was determined to originate primarily from neutron capture events in the EJ-301 detector volume.[6] As the neutrons enter the volume and interact with the hydrocarbon liquid scintillator and generate the luminescence that is used to detect the presence of the neutron, they also lose energy. When the neutrons slow to thermal energy they can be captured by the hydrogen and release gamma radiation. These gamma rays are then recorded by the system as a background. The spectrum quickly builds while neutrons are impinging on the detector and then exponentially decays in time. To determine this time-dependent portion of the background, simulations were run utilizing the Monte Carlo code MCNP (Ref. 12). The MCNP results were used to obtain the background shape and were then normalized to long TOFs, where essentially no primary neutrons originating from the neutron-producing target are detected. Figure 3 shows an example of the constant background, also known as room background, and the exponentially decaying portion of the neutron data and how the MCNP-simulated background connects the two regions under the peak of the primary neutron collection.

The uncertainty in the transmission was determined by propagating the individual uncertainties for each of the components in Eq. (1). Assuming uncorrelated errors, the uncertainty is given by

$$(\Delta T)^2 = \left(\frac{\partial T}{\partial C^S}\Delta C^S\right)^2 + \left(\frac{\partial T}{\partial C^O}\Delta C^O\right)^2 + \left(\frac{\partial T}{\partial B^S}\Delta B^S\right)^2 + \left(\frac{\partial T}{\partial B^O}\Delta B^O\right)^2 + \left(\frac{\partial T}{\partial mon^S}\Delta mon^S\right)^2 + \left(\frac{\partial T}{\partial mon^O}\Delta mon^O\right)^2 , \quad (2)$$

where

ΔT = 1σ uncertainty in the transmission

ΔC^S, ΔC^O = statistical uncertainties in the sample and open measurements, respectively

ΔB^S, ΔB^O = uncertainties in the sample and open backgrounds, respectively

Δmon^S, Δmon^O = uncertainties in the sample and open monitor counts, respectively.

In the TOF method the energy of the neutrons in each TOF channel collected by the P7889 clock is determined by relating the neutron energy to the neutron velocity. The velocity is calculated from the neutron generation time (zero time), the neutron detection time, and the flight

path distance. The neutron generation time can be calculated using the nearly instantaneous burst of gamma radiation emitted from the neutron target during neutron production, the gamma flash. The relation of the gamma flash to the neutrons detected can be seen in Fig. 3. Since the gamma radiation travels at the speed of light, the generation time can be calculated using the flight path distance. With neutron energies being recorded in the mega-electron-volt range, relativistic velocities were used in the TOF conversion as shown in Eq. (3):

$$E(t) = m_0c^2\left(\frac{1}{\sqrt{\left(1-\frac{d^2}{c^2t^2}\right)}}-1\right), \tag{3}$$

where

$E(t)$ = energy for TOF t

m_0c^2 = rest mass energy of a neutron

d = flight path distance

t = neutron TOF

c = speed of light in vacuum.

The uncertainty in the energy, defined as the ability to resolve the energy about a single TOF channel, was determined by propagating the uncertainties in each of the components in Eq. (3). This results in Eq. (4):

$$(\Delta E)^2 = \left(\frac{\partial E}{\partial t}\Delta t_{pw}\right)^2 + \left(\frac{\partial E}{\partial t}\Delta t_{cw}\right)^2 + \left(\frac{\partial E}{\partial d}\Delta d_{det}\right)^2 + \left(\frac{\partial E}{\partial d}\Delta d_{tar}\right)^2, \tag{4}$$

where

ΔE = uncertainty in the energy

Δt_{pw}, Δt_{cw} = uncertainty in time caused by the distribution of the linac pulse widths and the TOF clock channel width, respectively

Δd_{det}, Δd_{tar} = uncertainties in distance from the detector and target thickness, respectively.

The relation between the neutron transmission and the experimental total cross section is given by

$$\sigma_t(E) = -\frac{1}{N}\ln(T(E)), \tag{5}$$

where $\sigma_t(E)$ is the microscopic neutron total cross section of the sample and N is the sample areal number density in atoms/barn (1 barn = 10^{-24} cm^2). The uncertainty in the

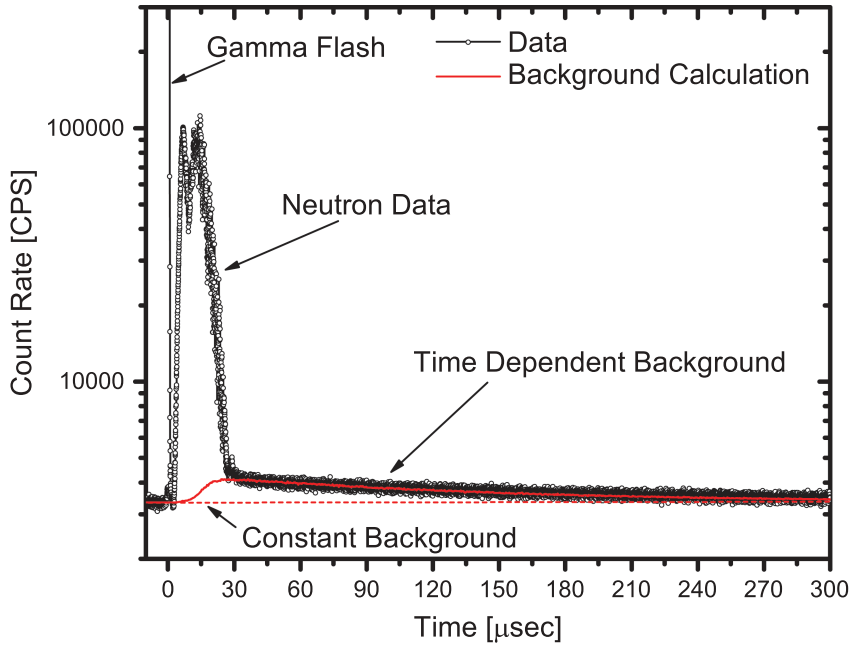

Fig. 3. The run-summed counting rate (data) and the MCNP-calculated background (solid red line). The red dashed line represents the constant room background. As shown, the calculated time-dependent background approaches the room background at long TOF.

experimental neutron total cross section $\Delta\sigma_t(E)$ was calculated using Eq. (6):

$$\Delta\sigma_t(E) = \left(\frac{1}{N}\right)\left(\frac{\Delta T(E)}{T(E)}\right) . \quad (6)$$

The uncertainty in N for such thick samples is very small compared to the statistical uncertainty associated with T and was therefore ignored.

III. RESULTS

III.A. Tantalum

Data were collected for two thicknesses of tantalum at a flight path distance of approximately 100 m. A 250-m flight path experiment was not performed for tantalum. The smooth cross section observed in the data did not warrant the separate measurement with the improved energy resolution of the longer flight path. The experimental neutron total cross section for the 5.5-cm thickness of tantalum is shown in Fig. 4; the two sample thicknesses generally agree to within 1% and are indistinguishable if plotted together at the scale shown. Although the data were recorded in 1.6-ns time bins, Fig. 4 presents the data grouped into bins of 51.2 ns/channel to decrease the statistical noise. Grouping the data causes a reduction in the statistical uncertainty by averaging the cross section over a number of data points. This reduction in statistical uncertainty introduces a reduction in energy resolution by increasing the time bins Δt_{cw} in Eq. (4). The three major nuclear data libraries, ENDF-8.0 (Ref. 13), JEFF-3.3 (Ref. 14), and JENDL-4.0 (Ref. 15), are shown for comparison.

A comparison to recent measurements pulled from the EXFOR database[16] is shown in Fig. 5. The Naval Nuclear Laboratory (NNL) and RPI data lie systematically below the data presented by Hannaske et al.[17] but largely within the measurement uncertainty in the energy range from 0.4 to 10 MeV. The NNL/RPI data agree within uncertainties with the work by Finlay et al.[18] for energies above 5 MeV.

For incident neutron energies of 0.4 to 2.0 MeV the ENDF-8.0 evaluation is above both the data presented in this work (NNL/RPI) and the evaluations of JEFF-3.3 and JENDL-4.0, with the JEFF-3.3 evaluation providing the best comparison to the data. For incident neutron energies between 2 and 7 MeV the ENDF-8.0 evaluation provides the best agreement with the NNL/RPI data where JEFF-3.3 and JENDL-4.0 trend low. For incident neutron energies greater than 7 MeV all three evaluations are generally below the NNL/RPI data with the JEFF-3.3 evaluation showing the best agreement. JEFF-3.3 is the

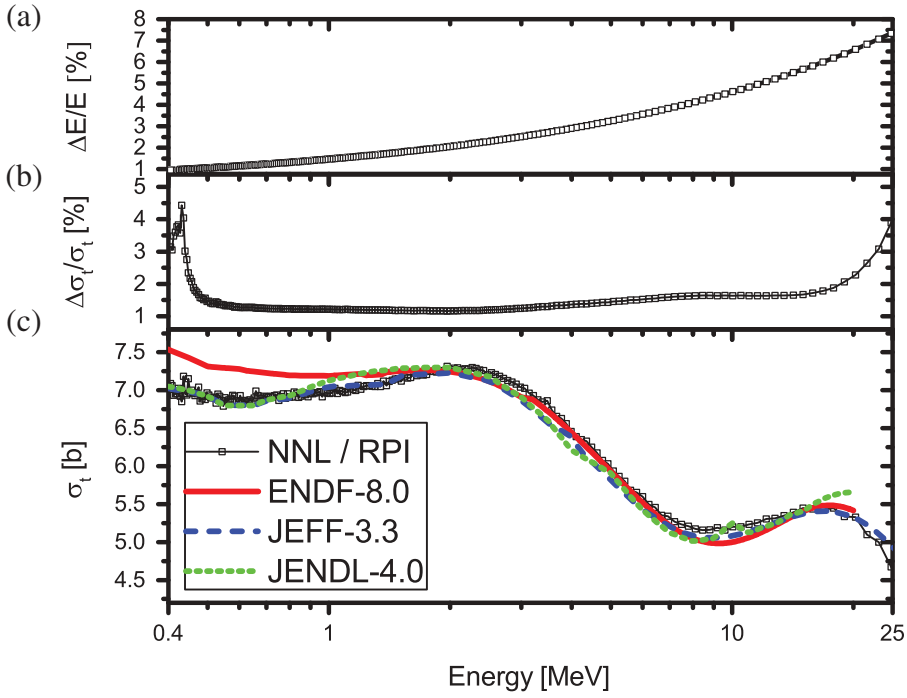

Fig. 4. The NNL/RPI neutron total cross section for tantalum data grouped to a TOF channel width of 51.2 ns/channel: (a) energy uncertainty, (b) uncertainty in the NNL/RPI data, and (c) compared with the ENDF-8.0, JEFF-3.3, and JENDL-4.0 nuclear data libraries over the energy range 0.4 to 25 MeV.

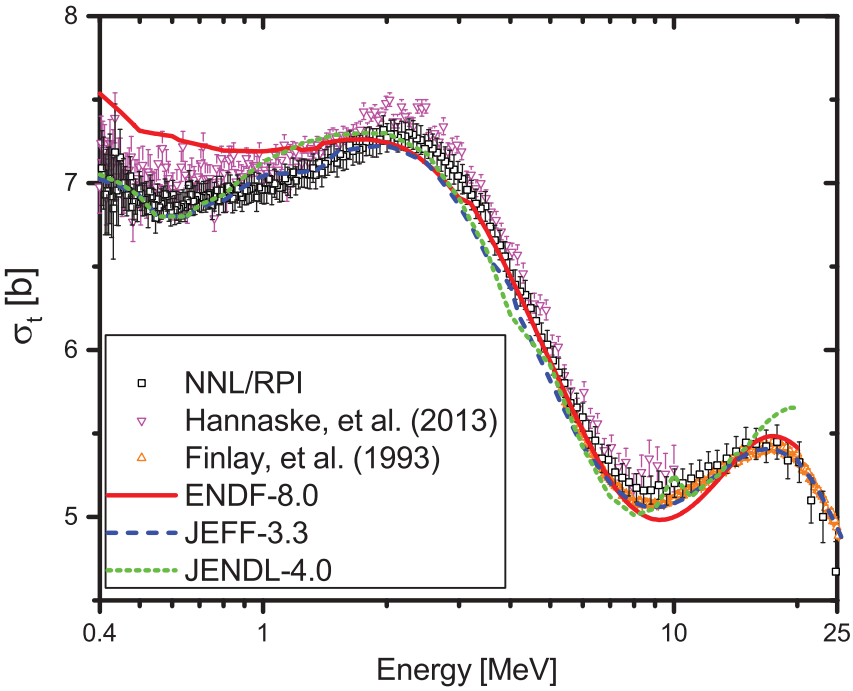

Fig. 5. The NNL/RPI neutron total cross section for tantalum data grouped to a TOF channel width of 51.2 ns/channel and compared to recent measurements (Hannaske, et al.[17] and Finlay et al.[18]) downloaded from the EXFOR database.[16]

only library that continues for neutron energies greater than 20 MeV.

III.B. Titanium

Data were collected for two thicknesses of titanium at flight path distances of approximately 100 and 250 m. Preliminary experiments were run at a flight path of 100 m. However, due to the observed structure in cross section below neutron energies of 5 MeV, 250-m data were collected to take advantage of the higher resolution at longer flight paths. Only the 250-m results are shown in Figs. 6 and 7. The measured cross sections for the two sample thicknesses for each of the flight paths agree within uncertainties, generally to within 1%. Titanium contains a large amount of structure in the neutron total cross section below 5 MeV. This structure is represented in the three nuclear data libraries shown in Figs. 6 and 7; however, the magnitude of the structure is greater in the NNL/RPI data than in any of the libraries. The ENDF-8.0 and JENDL-4.0 libraries provide resonance parameters for ^{50}Ti up to 587 keV, but below the measurement range of this work for all other isotopes. The resolved resonance region (RRR) ends below 300 keV for all isotopes in the JEFF-3.3 library. None of the libraries provide unresolved resonance parameters above the RRR for any isotope.

A comparison to measurements downloaded from the EXFOR database is shown in Fig. 8. The NNL/RPI data are in good agreement with Barnard et al.[19] for energies below 1.5 MeV and Cabe and Cance[20] for energies below 4 MeV; only a portion of this range is shown in Fig. 8 for image clarity. The NNL/RPI data provide better energy resolution and uncertainties than either measurement, as is evidenced by the sharper structure seen in the NNL/RPI cross section in Fig. 8. The NNL/RPI data also agree within uncertainty with the Abfalterer et al.[21] data for energies above 5 MeV.

For energies below 5 MeV all three nuclear data libraries show similar structure and have good agreement with the NNL/RPI data, although all three provide lower peak cross sections. For incident neutron energies between 5 and 12 MeV the JEFF-3.3 and JENDL-4.0 libraries show the best agreement and ENDF-8.0 and JEFF-3.3 have the best agreement for energies above 12 MeV. JEFF-3.3 is the only library that continues for neutron energies greater than 20 MeV.

III.C. Zirconium

Data were collected for two thicknesses of zirconium at flight path distances of approximately 100 and 250 m. The data show that zirconium contains a large amount of structure in the total cross section below 2.5 MeV, a region

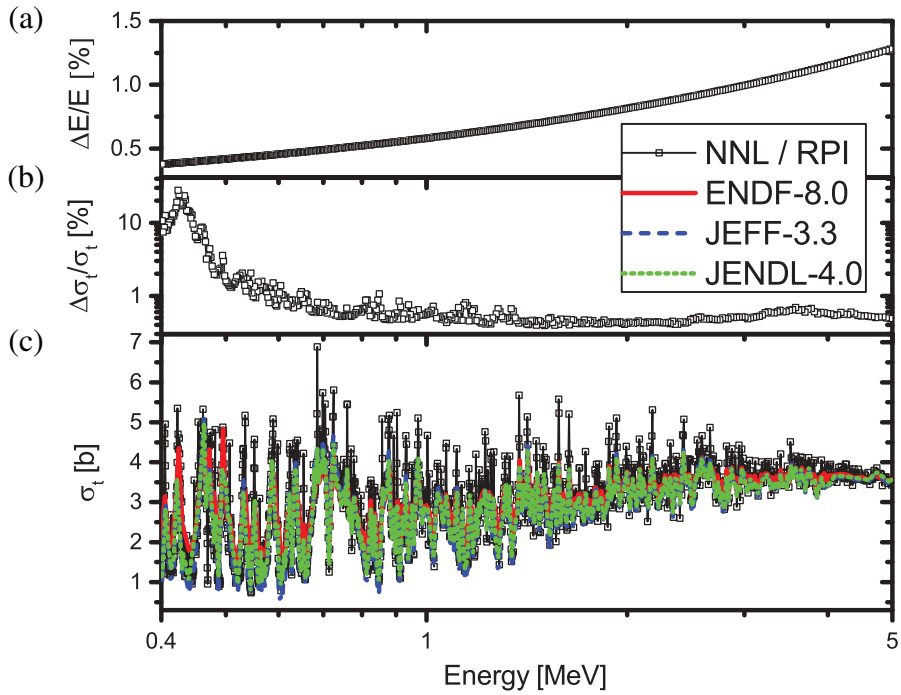

Fig. 6. The NNL/RPI neutron total cross section for titanium data grouped to a TOF channel width of 12.8 ns/channel: (a) energy uncertainty, (b) uncertainty in the NNL/RPI data, and (c) compared to the ENDF-8.0, JEFF-3.3, and JENDL-4.0 nuclear data libraries over the energy range 0.4 to 5 MeV.

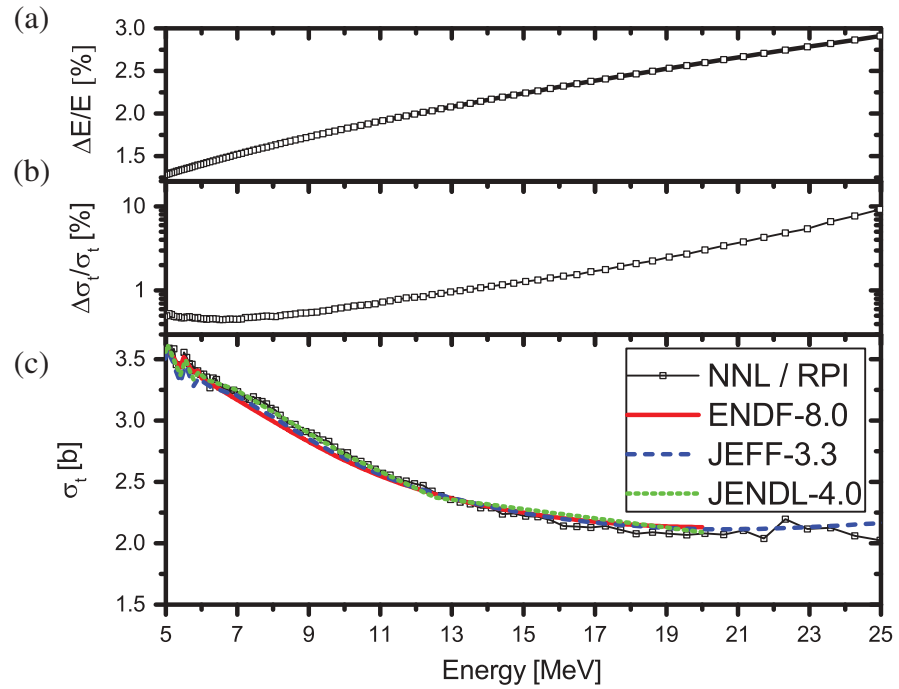

Fig. 7. The NNL/RPI neutron total cross section for titanium data grouped to a TOF channel width of 51.2 ns/channel: (a) energy uncertainty, (b) uncertainty in the NNL/RPI data, and (c) compared to the ENDF-8.0, JEFF-3.3, and JENDL-4.0 nuclear data libraries over the energy range 5 to 25 MeV.

of this (0.75 to 1.75 MeV) is shown in Fig. 9. This structure is not represented in the three nuclear data libraries; however, the ENDF-8.0 library provides unresolved resonance parameters for the isotopes of zirconium up to approximately 1.7 MeV for ^{90}Zr and ^{96}Zr, and 1 MeV for ^{91}Zr, ^{92}Zr, and ^{94}Zr. The measured cross section for the two

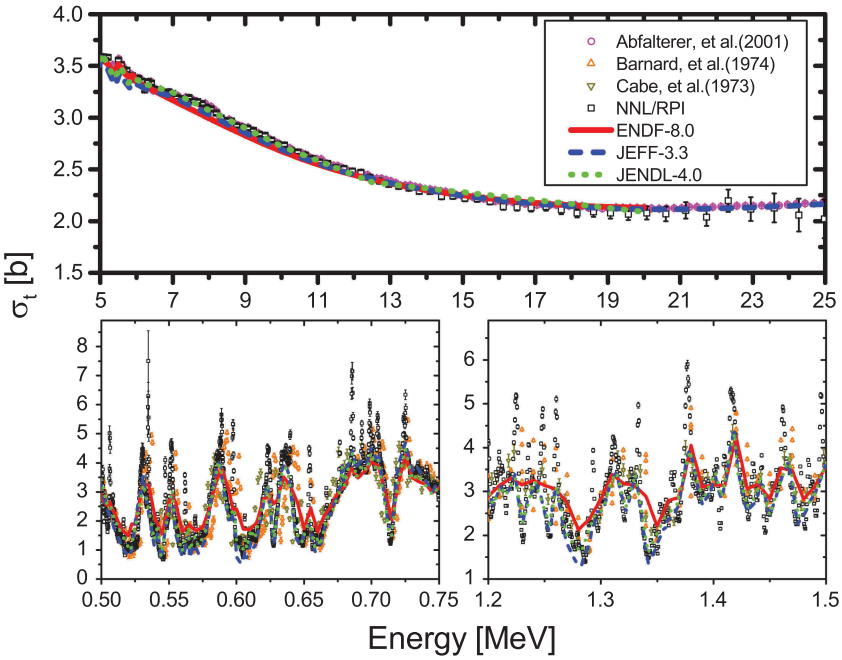

Fig. 8. The NNL/RPI neutron total cross section for titanium data compared to measurements downloaded from the EXFOR database[16]: Abfalterer et al.,[21] Barnard et al.,[19] and Cabe and Cance.[20]

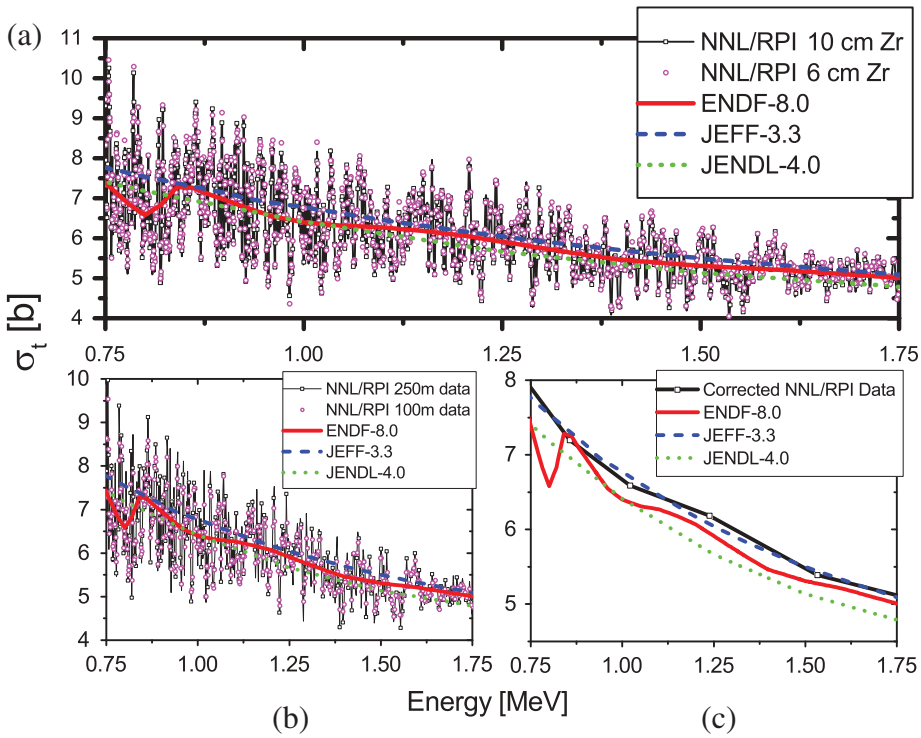

Fig. 9. The NNL/RPI neutron total cross section for zirconium data compared to the nuclear data libraries over the energy range 0.75 to 1.75 MeV. (a) The top figure compares data collected at 250 m in 3.2 ns/channel, showing agreement between the 10- and 6-cm Zr samples. (b) Comparison of data collected at 250 m in 51.2 ns/channel and 100 m in 3.2 ns/channel, showing agreement between the 250- and 100-m measurements. (c) The NNL/RPI data corrected for sample self-shielding using the Fröhner et al. method.[22]

sample thicknesses for each of the flight paths generally agree to within 1%. Due to the large amount of structure seen in the cross section and the smooth cross section observed in the evaluations an investigation into the resolution self-shielding effect described by Fröhner et al.[22] was undertaken. This method utilizes two sample

thicknesses to correct for resolution effects in energy-averaged cross section, where the energy averaging smooths many large fluctuations in cross sections. The conclusion was an increase in the smoothed cross section below 1.75 MeV on the order of 1% to 2%, which places the Fröhner-corrected NNL/RPI data above the ENDF-8.0 and JENDL-4.0 libraries and close to the JEFF-3.3 library.

None of the natural zirconium data pulled from the EXFOR database presented the structure seen in the NNL/RPI data; however, the smoothed NNL/RPI data agree with the Poenitz and Whalen[23] data throughout the measured energy range within the measurement uncertainties. Measurements conducted on the primary isotope of zirconium, ^{90}Zr (51.5%), by Musgrove et al.[24] and Green and Mitchell[25] provide some information on the structure seen in the cross section with the NNL/RPI data showing structure at common energies as in their data. The comparison is shown in Fig. 10.

Of the three nuclear data libraries shown, the ENDF-8.0 library generally shows the best agreement with the NNL/RPI data throughout the measured range. The ENDF-8.0 library shows some deviation from the flat cross section seen in the other libraries below 1 MeV, which follows the smoothed NNL/RPI data with the TOF channels binned to 204.8 ns/channel as shown in Fig. 11. Below 2.5 MeV the ENDF-8.0 library does not provide the magnitude of structure seen in the NNL/RPI data but does represent the trend in cross section, in addition to providing unresolved resonance parameters below 1.7 MeV. The JEFF-3.3 library provides an accurate representation of the cross section if the NNL/RPI data were further smoothed below 2.5 MeV, but is low compared to the NNL/RPI data in the range of 5 to 10 MeV. The JENDL-4.0 library is below the NNL/RPI data less than 2.5 MeV, even when smoothed, and is above the NNL/RPI data for neutron energies between 2.5 and 7 MeV. The JEFF-3.3 library ends the unresolved resonance region (URR) at 100 keV and the JENDL-4.0 library ends the URR less than 400 keV for all isotopes of zirconium. JEFF-3.3 is the only library that continues for neutron energies greater than 20 MeV.

IV. CONCLUSIONS

This paper presents new high-resolution measurements of tantalum, titanium, and zirconium, and compares the measured data to commonly used nuclear data evaluations for neutron total cross sections. Each of the measurements provided indicate that improvements can be made in the nuclear data evaluations. Figure 12 provides an overall

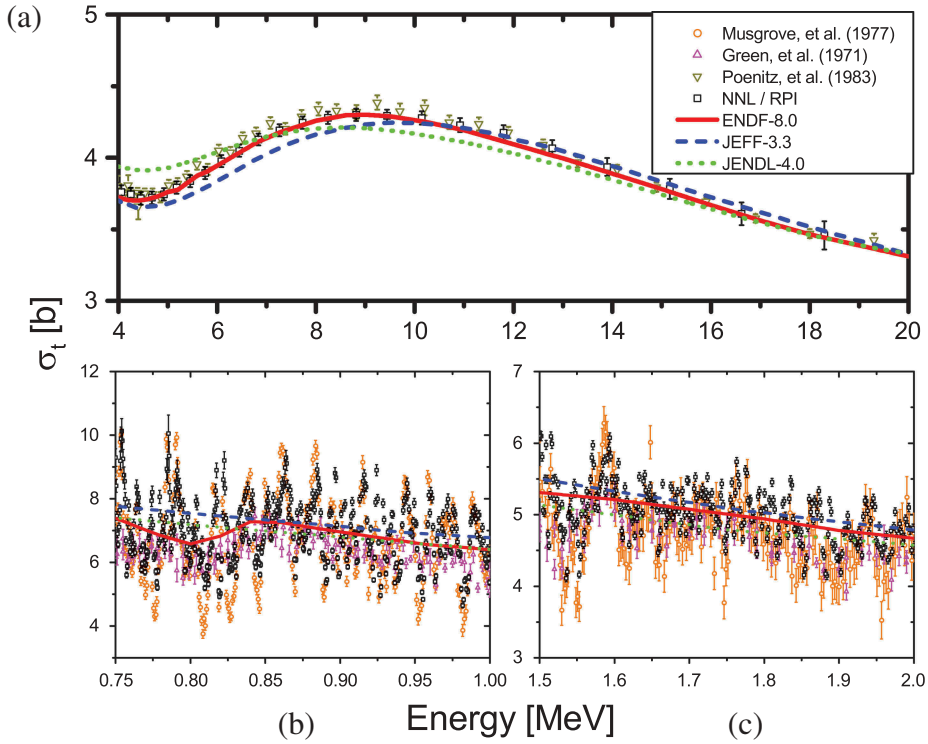

Fig. 10. The NNL/RPI neutron total cross section for zirconium compared to measurements downloaded from the EXFOR database[16]: Musgrove et al.,[24] Green and Mitchell,[25] and Poenitz and Whalen.[23] (a) The data from Poenitz and Whalen are from natural samples, while the data from (b) Green and Mitchell and (c) Musgrove et al. are from ^{90}Zr measurements.

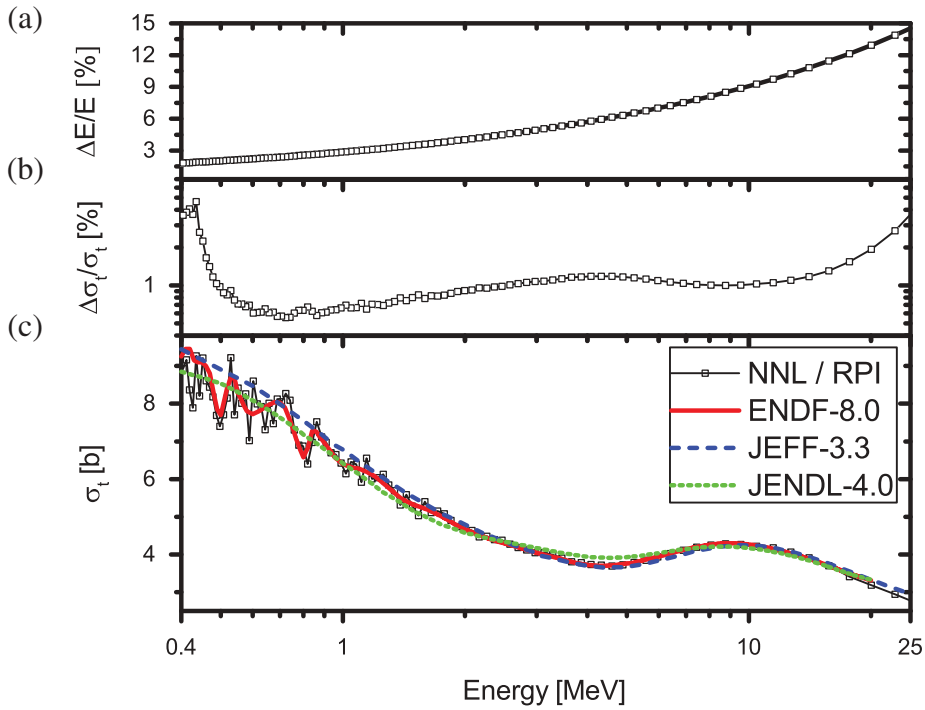

Fig. 11. The NNL/RPI neutron total cross section for zirconium data grouped to a TOF channel width of 204.8 ns/channel: (a) energy uncertainty, (b) uncertainty in the NNL/RPI data, and (c) compared to the ENDF-8.0, JEFF-3.3, and JENDL-4.0 nuclear data libraries over the energy range 0.4 to 5 MeV.

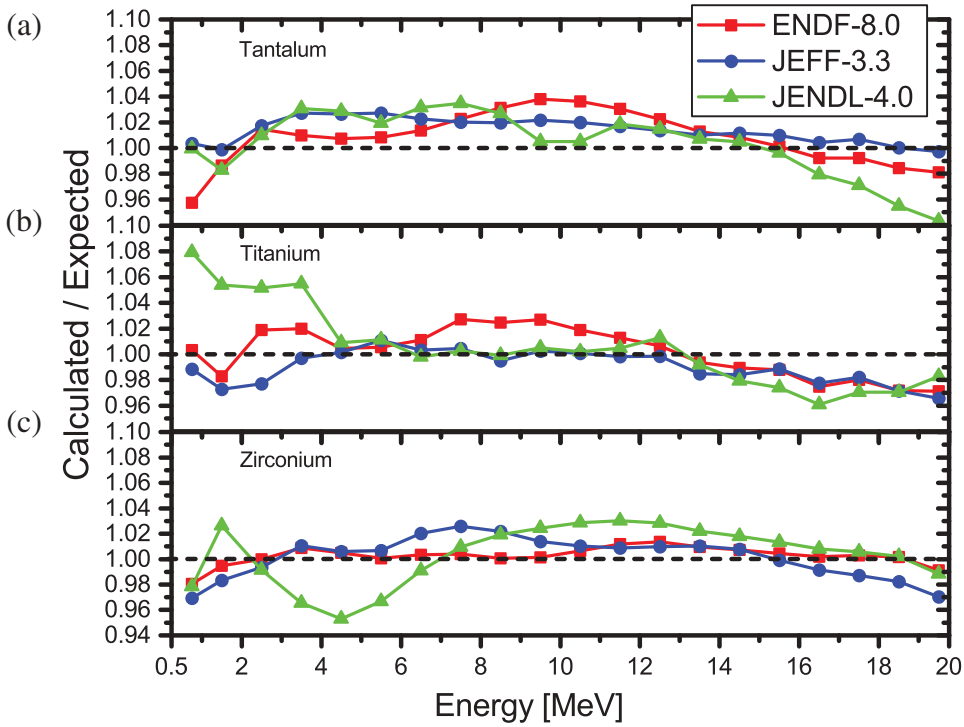

Fig. 12. The ratio of calculated (NNL/RPI data) to expected (ENDF-8.0, JEFF-3.3, and JENDL-4.0 nuclear data libraries) for (a) tantalum, (b) titanium, and (c) zirconium.

view of the differences between the total neutron cross section in energy regions of 1 MeV, with the exception of the first bin (0.5 to 1 MeV), between the NNL/RPI data and the nuclear data libraries by using a ratio of the calculated (NNL/RPI data) and expected (nuclear data library) for each of the materials measured. The tantalum measurement

showed a large discrepancy with the current ENDF-8.0 evaluation below 2 MeV and with JENDL-4.0 above 15 MeV. The JEFF-3.3 evaluation generally showed good agreement with the NNL/RPI data through the measured energy range. The titanium measurement generally agreed with the current neutron total cross-section evaluations through the energy range measured. However, some discrepancies were noted in the structure seen in the cross section in the 0.4- to 4-MeV energy range. Measurements of the zirconium neutron total cross section are generally higher than the evaluations in the 2- through 7-MeV range. Structure was also seen in the zirconium neutron total cross section that is not addressed in the JEFF-3.3 and JENDL-4.0 libraries, while the ENDF-8.0 library extends the URR to between 1 and 1.7 MeV for the isotopes of zirconium. The presented work identifies regions where neutron total cross sections could be improved in future evaluations. As such, the neutron total cross-section measurements presented here could help nuclear data evaluators improve neutron total cross-section data in future evaluations.

Acknowledgments

The submitted manuscript has been authored by a contractor of the U.S. Government under contract no. DE-NR-0000031. Accordingly, the U.S. Government retains a nonexclusive, royalty-free license to publish or reproduce the published form of this contribution, or allow others to do so, for U.S. Government purposes. The authors would like to thank the Gaerttner Linear Accelerator Center operators and staff: P. Brand, M. Gray, A. Kerdoun, L. Krusieski, and M. Strock, without whom these experiments could not have been performed.

References

1. F. BROSSA, G. PIATTI, and M. BARDY, "Tantalum Protective Coatings for Fusion Reactor Applications," *J. Nucl. Mater.*, **103**, 261 (2000); https://doi.org/10.1016/0022-3115(82)90608-0.
2. L. LEAL et al., "Assessment of Titanium Cross Sections and Uncertainties for Application in Criticality Safety," *Proc. 8th Int. Conf. on Nuclear Criticality* Safety *(ICNC 2007)* (2007).
3. R. T. WEBSTER, "Zirconium for Nuclear Primary Steam Systems," *ASTM Int. STP Ser.*, **551**, 5 (1974).
4. M. E. OVERBURG et al., "Photoneutron Target Development for the RPI Linear Accelerator," *Nucl. Instrum. Methods Phys. Res. A*, **438**, 254 (1999).
5. F. J. SAGLIME, "High Energy Nuclear Differential Scattering Measurements for Beryllium and Molybdenum," PhD Thesis, Rensselaer Polytechnic Institute (2009).
6. M. J. RAPP et al., "Beryllium and Graphite Neutron Total Cross Section Measurements from 0.4 to 20 MeV," *Nucl. Sci. Eng.*, **172**, 268 (2012); https://doi.org/10.13182/NSE11-55.
7. *User Manual: P7889 100ps/10 GHz Time-of-Flight /Multiscaler*, FAST ComTec GmbH, Oberhaching, Germany (2006).
8. Y. DANON and R. C. BLOCK, "Minimizing the Statistical Error of Resonance Parameters and Cross Sections Derived from Transmission Measurements," *Nucl. Instrum. Methods Phys. Res. A*, **485**, 585 (2002); https://doi.org/10.1016/S0168-9002(01)02118-0.
9. Y. DANON et al., "Beryllium and Graphite High-Accuracy Total Cross Section Measurements in the Energy Range from 34 to 900 keV," *Nucl. Sci. Eng.*, **161**, 321 (2009); https://doi.org/10.13182/NSE161-321.
10. Y. DANON, *Rensselaer Polytechnic Institute Cross Section Data Reduction Computer Code (RPIXDR 2.2.2)*, Rensselaer Polytechnic Institute, Troy, New York (2006).
11. Y. DANON, "Design and Construction of the RPI Enhanced Thermal Neutron Target and Thermal Cross Section Measurements of Rare Earth Elements," PhD Thesis, Rensselaer Polytechnic Institute (1993).
12. X-5 MONTE CARLO TEAM, "MCNP—A General Monte Carlo N-Particle Transport Code, Version 5," LA-UR-03-1987, Los Alamos National Laboratory (2003, Rev. 2008).
13. D. A. BROWN et al., "ENDF/B-VIII.0: The 8th Major Release of the Nuclear Reaction Data Library with CIELO-Project Cross Sections, New Standards and Thermal Scattering," *Nucl. Data Sheets*, **148**, 1 (2018); https://doi.org/10.1016/j.nds.2018.02.001.
14. "The Joint Evaluated Fission and Fusion File (JEFF)," Organisation for Economic Co-operation and Development/Nuclear Energy Agency; www.oecd-nea.org/dbdata/jeff/jeff33/ (accessed June 30, 2018).
15. K. SHIBATA et al., "JENDL-4.0: A New Library for Nuclear Science and Engineering," *J. Nucl. Sci. Technol.*, **48**, 1 (2011); https://doi.org/10.1080/18811248.2011.9711675.
16. V. SEMKOVA et al., "EXFOR—A Global Experimental Nuclear Reaction Data Repository: Status and New Developments," ND2016: Int. Conf. on Nuclear Data for Science and Technology, Vol. 146, EPJ Web Conf. (2017).
17. R. HANNASKE et al., "Neutron Total Cross Section Measurements of Gold and Tantalum at the nELBE

Photoneutron Source," *Eur. Phys. J. A*, **49**, 137 (2013); https://doi.org/10.1140/epja/i2013-13137-1.

18. R. W. FINLAY et al., "Neutron Total Cross Sections at Intermediate Energies," *Phys. Rev. Part C Nucl. Phys.*, **47**, 237 (1993); https://doi.org/10.1103/PhysRevC.47.237.
19. E. BARNARD et al., "Neutron Scattering from Titanium; Compound and Direct Effects," *Nucl. Phys. Sec. A*, **229**, 189 (1974); https://doi.org/10.1016/0375-9474(74)90782-9.
20. J. CABE and M. CANCE, "Measurements of the Neutron Total Cross Sections of Be, B-11, C, Al, Si, S, Ti, V, Ni, U-235, U-238, Pu-239 Between 100 keV and 6 MeV," Saclay Reports Number 4524, CEA/DAM, Centre d'Etudes Nucleaires (1973).
21. W. P. ABFALTERER et al., "Measurement of Neutron Total Cross Sections up to 560 MeV," *Phys. Rev. Part C Nucl. Phys.*, **63**, 044608 (2001); https://doi.org/10.1103/PhysRevC.63.044608.
22. F. FRÖHNER et al., "Cross-Section Fluctuations and Self-Shielding Effects in the Unresolved Resonance Region," International Evaluation Co-operation, Vol. 15 (NEA-WPEC-15), Organisation for Economic Co-operation and Development/Nuclear Energy Agency (1995).
23. W. P. POENITZ and J. F. WHALEN, "Neutron Total Cross Section Measurements in the Energy Range from 47 KeV to 20 MeV," ANL-NDM Number 80, Argonne National Laboratory Reports (1983).
24. A. R. D. L. MUSGROVE, J. A. HARVEY, and W. M. GOOD, "Neutron Resonance Parameters of ^{90}Zr Below 300 keV," *Aust. J. Phys.*, **30**, 379 (1977); https://doi.org/10.1071/PH770379.
25. L. GREEN and J. MITCHELL, "Total Cross Section Measurements with a ^{252}Cf Time-of-Flight Spectrometer," 3rd Conf. Neutron Cross-Sections+Tech., Knoxville, Tennessee, Vol. 1, p. 325 (1971).